CHAPTER IV.

FREE VIBRATION PROBLEM

4.1 Overview

For the problem at hand, the induced elastic couplings must play a decisive role in the enhancement of the free vibraion and forced response characteristics of wing structures. At the same time, the selected ply-angle orientation should not generate undesired couplings, producing unwanted effects on the response characteristics. In this case, the bending-twist coupling is most important in the design of aircraft wings.

As shown previously (see Chapter 3), the ply-angle distribution with respect to the spanwise z - axis inducing such a cross-coupling is

$$\theta(y) = -\theta(-y) \tag{4.1}$$

The corresponding boundary-value problem can be derived by means of the extended Hamilton's principle [44], which, for the problem at hand, is obtainable from Eq. (2.6.1) as

$$\int_{t_1}^{t_2} \left(\delta T - \delta V + \delta W\right) dt = 0, \quad \delta v_o = \delta\theta_x = \delta\varphi = 0 \qquad \text{at } t = t_1, t_2 \tag{4.2}$$

where all the variables have been already defined. From Eq. (2.4.1), the kinetic energy is reduced to

$$T = \frac{1}{2}\int_0^L \oint \sum_{k=1}^{N} \int_{h(k)} \rho^{(k)} \Big[(y\dot{\varphi})^2 + (\dot{v}_o + x\dot{\varphi})^2 + \Big\{ (y\dot{\theta}_x - F_w\dot{\varphi}') - n\left(\frac{dx}{ds}\dot{\theta}_x + a\dot{\varphi}'\right) \Big\}^2 \Big] dn ds dz \tag{4.3}$$

and from Eq. (2.4.3), the corresponding potential energy has the form

$$V = \frac{1}{2}\int_0^L \oint \sum_{k=1}^{N} \int_{h(k)} \Big\{ \sigma_{zz}^{(k)} \Big[y\theta_x' - F_w\varphi'' - n\left(\frac{dx}{ds}\theta_x' + a\varphi''\right) \Big] + \sigma_{sz}^{(k)} \Big[(v_o' + \theta_x)\frac{dy}{ds} + \frac{2A_C}{\beta}\varphi' \Big] - \sigma_{nz}^{(k)} (v_o' + \theta_x)\frac{dx}{ds} \Big\} dn ds dz \tag{4.4}$$

Moreover, the virtual work can be written as

$$\delta W = \int_0^L \left[p_y(z,t)\delta v_o(z,t) + m_z(z,t)\delta\varphi(z,t) \right] dz + M_x^a \delta\theta_x(L,t) \tag{4.5}$$

where p_y and m_z are the external force per unit length and twist moment about the z axis, respectively. Carrying out the integration of Eq. (4.3) with respect to n and introducing

mass terms m_i displayed in Appendix A, the kinetic energy can be expressed in the form as:

$$T = \frac{1}{2}\int_0^L \Big\{ m_o\Big[\Big(y\dot{\varphi}\Big)^2 + \Big(\dot{v}_o + x\dot{\varphi}\Big)^2 + \Big(y\dot{\theta}_x - F_w\dot{\varphi}'\Big)^2 - 2n\Big(y\dot{\theta}_x - F_w\dot{\varphi}'\Big)$$

$$\left(\frac{dx}{ds}\dot{\theta}_x + a\dot{\varphi}'\right)^2 + m_2\left(\frac{dx}{ds}\dot{\theta}_x + a\dot{\varphi}'\right)^2\Big] ds\, dz \tag{4.6a}$$

In addition, integration of Eq. (4.6a) with respect to s in conjuction with definitions of reduced mass terms, b_i and geometric conditions, Eq. (3.2a) yields

$$T = \frac{1}{2}\int_0^L \Big[b_1(\dot{v}_o)^2 + (b_4 + b_5)(\dot{\varphi})^2 + (b_{10} + b_{18})(\dot{\varphi}')^2 + (b_4 + b_{14})(\dot{\theta}_x)^2\Big] dz \tag{4.6b}$$

where the various coefficients are displayed in the Appendix A. Integration of Eq. (4.4) with respect to n and s, results in an alternate expression of the potential energy given by:

$$V = \frac{1}{2}\int_0^L \left[M_x\theta_x' + Q_y(\theta_x + v_o') - B_w\varphi'' + M_z\varphi'\right] dz$$

$$= \frac{1}{2}\int_0^L \Big[a_{33}(\theta_x')^2 + a_{55}(\theta_x)^2 + a_{66}(\varphi'')^2 + a_{77}(\varphi')^2 + a_{55}(v_o')^2 + 2a_{37}\theta_x'\varphi'$$

$$+2a_{55}v_o'\theta_x + 2a_{56}\theta_x\varphi'' + 2a_{56}v_o'\varphi''\Big] dz \tag{4.7}$$

The stiffness quantities appearing in Eq. (4.7) are displayed in the Appendix A.

4.2 The Discretized Equations of Motion of Cantilevers Featuring Bending-Twist Coupling

For practical reasons, it is necessary to discretize the boundary-value problem, which amounts to representing v_o, θ_x and φ by means of series of space-dependent trial functions multiplied by time-dependent generalized coordinates. The discretization can be more conveniently performed directly in the extended Hamilton's principle [54]. To this end, we express the displacements v_o, θ_x and φ as follows:

$$v_o(z,t) = \underline{\phi_1}^T(z)\underline{\boldsymbol{q}_1}(t), \quad \theta_x(z,t) = \underline{\phi_2}^T(z)\underline{\boldsymbol{q}_2}(t), \quad \varphi(z,t) = \underline{\phi_3}^T(z)\underline{\boldsymbol{q}_3}(t) \tag{4.8a-c}$$

where $\underline{\phi_1} = \left[\phi_1\ \phi_2 \quad \phi_N\right]^T$, $\underline{\phi_2} = \left[\phi_{N+1}\ \phi_{N+2} \quad \phi_{2N}\right]^T$, $\underline{\phi_3} = \left[\phi_{2N+1}\ \phi_{2N+2} \quad \phi_{3N}\right]^T$ are vectors of suitable trial functions, while $\underline{\boldsymbol{q}_1} = \left[q_1\ q_2 \quad q_N\right]^T$, $\underline{\boldsymbol{q}_2} = \left[q_{N+1}\ q_{N+2} \quad q_{2N}\right]^T$, $\underline{\boldsymbol{q}_3} = \left[q_{2N+1}\ q_{2N+2} \quad q_{3N}\right]^T$ are vectors of generalized coordinates. In the forthcoming developments, the underbars will be omitted. Then, inserting Eq. (4.8) into Eq. (4.6b), we can write the kinetic energy in discretized form as

$$T = \frac{1}{2}\dot{\boldsymbol{q}}^T\boldsymbol{M}\dot{\boldsymbol{q}} \tag{4.9}$$

where

$$\boldsymbol{M} = \int_0^L \begin{bmatrix} b_1\phi_1\phi_1^T & \mathbf{0} & \mathbf{0} \\ \mathbf{0} & (b_4 + b_{14})\phi_2\phi_2^T & \mathbf{0} \\ \mathbf{0} & \mathbf{0} & (b_4 + b_5)\phi_3\phi_3^T + (b_{10} + b_{18})\phi_3'\phi_3'^T \end{bmatrix} dz \tag{4.10}$$

is the corresponding mass matrix. Herein $\boldsymbol{q} = \left[\underline{\boldsymbol{q}}_1^T \; \underline{\boldsymbol{q}}_2^T \; \underline{\boldsymbol{q}}_3^T\right]^T$ is the overall generalized displacement vector and $\mathbf{0}$ is null matrix of appropriate dimension.
Similarly, using Eq. (4.7), we obtain the discretized potential energy

$$V = \frac{1}{2}\boldsymbol{q}^T \boldsymbol{K} \boldsymbol{q} \tag{4.11}$$

where

$$\boldsymbol{K} = \int_0^L \begin{bmatrix} a_{55}\phi_1'\phi_1'^T & a_{55}\phi_1'\phi_2^T & a_{56}\phi_1'\phi_3''^T \\ & a_{55}\phi_2\phi_2^T + a_{33}\phi_2'\phi_2'^T & a_{37}\phi_2'\phi_3'^T + a_{56}\phi_2\phi_3''^T \\ \textit{symm} & & a_{77}\phi_3'\phi_3'^T + a_{66}\phi_3''\phi_3''^T \end{bmatrix} dz \tag{4.12}$$

is the corresponding stiffness matrix.

Before we can discretize the virtual work, we recall from Eq. (3.11) that the boundary moment control has the expression

$$M_x^a = k_V \dot{\theta}_x(L,t) + k_A \ddot{\theta}_x(L,t) \tag{4.13}$$

Inserting Eqs. (4.8) and (4.13) into Eq. (4.5), the discretized virtual work can be expressed in the form

$$\delta W = \boldsymbol{Q}^T \delta\boldsymbol{q} - \dot{\boldsymbol{q}}^T \boldsymbol{H} \delta\boldsymbol{q} - \ddot{\boldsymbol{q}}^T \boldsymbol{E} \delta\boldsymbol{q} \tag{4.14}$$

in which

$$\boldsymbol{Q} = \int_0^L \begin{bmatrix} p_y\phi_1^T & \mathbf{0}^T & m_z\phi_3'^T \end{bmatrix}^T dz \tag{4.15}$$

is a generalized force vector and

$$\boldsymbol{H} = \begin{bmatrix} \mathbf{0} & \mathbf{0} & \mathbf{0} \\ \mathbf{0} & k_V\phi_2(L)\phi_2'^T(L) & \mathbf{0} \\ \mathbf{0} & \mathbf{0} & \mathbf{0} \end{bmatrix} \tag{4.16}$$

$$\boldsymbol{E} = \begin{bmatrix} \mathbf{0} & \mathbf{0} & \mathbf{0} \\ \mathbf{0} & k_A\phi_2(L)\phi_2'^T(L) & \mathbf{0} \\ \mathbf{0} & \mathbf{0} & \mathbf{0} \end{bmatrix} \tag{4.17}$$

are coefficient matrices.

Replacement of Eqs. (4.9), (4.11) and (4.14) in Eq. (4.2), integrating the term involving $\delta\dot{\boldsymbol{q}}$ by parts with respect to time and recognizing the arbitrariness of $\delta\boldsymbol{q}$, we obtain the discretized equations of motion

$$\boldsymbol{M}^{*}\ddot{\boldsymbol{q}}(t) + \boldsymbol{H}\dot{\boldsymbol{q}}(t) + \boldsymbol{K}\boldsymbol{q}(t) = \boldsymbol{Q}(t) \tag{4.18a}$$

where M^{*} is a modified mass matrix,

$$\boldsymbol{M}^{*} = \boldsymbol{M} + \boldsymbol{E} \tag{4.18b}$$

4.3 State-Space Formulation

A solution of Eq. (4.18a) can be obtained conveniently by casting it first in the state-space form. To this end, we introduce the state vector $\boldsymbol{X} = \left[\boldsymbol{q}^{T}\ \dot{\boldsymbol{q}}^{T}\right]^{T}$ and adjoin the identity $\dot{\boldsymbol{q}} = \dot{\boldsymbol{q}}$. Then, the desired state form is

$$\dot{\boldsymbol{X}}(t) = \boldsymbol{A}\boldsymbol{X}(t) + \boldsymbol{B}\boldsymbol{Q}(t) \tag{4.19}$$

where

$$\boldsymbol{A} = \begin{bmatrix} \mathbf{0} & \mathbf{I} \\ -\boldsymbol{M}^{*-1}\boldsymbol{K} & -\boldsymbol{M}^{*-1}\boldsymbol{H} \end{bmatrix}, \quad \boldsymbol{B} = \begin{bmatrix} \mathbf{0} \\ \boldsymbol{M}^{*-1} \end{bmatrix} \tag{4.20}$$

are coefficient matrices, $\mathbf{0}$ and $\mathbf{I}$ denote, respectively, the null matrix and the identity matrix of appropriate dimensions.

4.4 Free Vibration Problem

Herein the eigenvalue problem associated with the system of equations (4.19) will be obtained. To this end, the homogenous solution of Eq. (4.19) is expressed as

$$\boldsymbol{X}(t) = \boldsymbol{x}\,e^{\lambda t} \tag{4.21}$$

in which $\boldsymbol{x}$ is a constant vector and λ a constant scalar, both generally complex valued quantities. Inserting Eq. (4.21) into Eq. (4.19) with $\boldsymbol{Q} = \mathbf{0}$, we obtain the eigenvalue problem

$$\boldsymbol{A}\boldsymbol{x} = \lambda\boldsymbol{x} \tag{4.22}$$

which can be solved for the eigenvalues λ_r and eigenvectors x_r ($r = 1,2,\ \ ,6N$). The top half of the eigenvectors can be used to replace $\boldsymbol{q}_{\mathrm{i}}$ in Eqs. (4.8) so as to obtain eigenfunctions. The corresponding eigenfunctions are displayed in Appendix D. The solution of the algebraic eigenvalue problem yields the closed-loop eigenvalues

$$\begin{Bmatrix} \lambda_r \\ \bar{\lambda}_r \end{Bmatrix} = \sigma_r \pm i\omega_{dr} \tag{4.23}$$

where σ_r is a measure of the damping in the r th mode and ω_{dr} is the r th frequency of damped oscillation. They depend on the feedback control gains k_V, k_A, the ply angle θ,

and the system parameters. From Eq. (4.23), we obtain the damping factor in the r th mode in the form

$$\zeta_r = -\frac{\sigma_r}{\sqrt{\sigma_r^2 + \omega_{dr}^2}} \tag{4.24}$$

We shoud remark that if an eigensolution λ_r, x_r is complex, then the complex conjugate pair $\bar{\lambda}_r$, $\bar{x}_r$ is also an eigensolution. Because λ appears in both the equations of motion and the boundary conditions, the solution of the corresponding eigenvalue problem tends to be complicated. Towards its solution, a MATHEMATICA software [55] in which symbolic manipulations are available, has been utilized.

The following numerical illustrations concern the eigenvalue problem of a cantilevered thin-walled beam of a biconvex cross-section profile. The geometric dimensions are displayed in Fig. 4.1 and the piezoactuator is made of PZT-4 ceramic, whose properties can be found in Appendix C.

In the numerical examples two materials are considered. One of them is the graphite epoxy material whose on-axis properties are displayed in Appendix B.

The second material has transversely-isotropic properties, the surface of isotropy being parallel at each point to the mid-surface of the beam. Due to its outstanding thermomechanical properties, this material (known as pyrolitic-graphite and its alloys) has all the chances to be used in the structure of high-speed flight vehicles. The elastic constants of its constituent material are displayed in Appendix B.

Figures 4.2(a) and 4.2(b) show plots of the ratio ω_{dr}/ω_r versus the nondimensional velocity feedback gain $K_V = k_V L\bar{\omega}/a_{33}$ for the first two modes and for the ply-anlge $\theta = 45^o$, in which ω_r is the frequency of undamped oscillation corresponding to the uncontrolled structure, and $\bar{\omega} = 44.50\ rad/s$ is an open-loop frequency corresponding to a free-warping, non-shearable beam model with $\theta = 0^o$ and $AR = 16$. The plots show that the effect of the feedback control is smaller for the second mode than for the first. Figure 4.3 depicts damping factor ζ in the first mode versus the ply angle θ for three different values of the velocity feedback gain K_V. The displayed results are for an unshearable beam of $AR = 16$ featuring warping restraint. In addition to the well-established fact that damping can be induced by feedback control, the plot reveals that structural tailoring can be used to increase damping in the structure as well.

Figures 4.4(a), 4.4(b) and 4.4(c) depict the first two damped eigenfrequencies versus the normalized velocity feedback gain K_V for various transverse shear flexibility ratios E/G', including the unshearable case ($E/G' = 0$), which corresponds to the Euler-Bernoulli beam model. In the expression of K_V, $\bar{\omega} = 128.16\ rad/s$ is the fundamental natural frequency of the unactivated beam characterized by $AR = 16$ and $E/G' = 50$.

In addition to the efficiency of the adopted control methodology to increase the closed loop eigenfrequencies, the results reveal also that use of the classical Euler-Bernoulli model results in overestimations of the natural frequencies. Whereas Figs. 4.4(a) and 4.4(b) reveal that an increase in the aspect ratio of the beam $AR(\equiv 2L/c)$, reduces the sensitivity of the frequencies to transverse shear effecs, Fig. 4.4(c) shows that transverse shear flexibility plays a more significant role in the case of larger mode frequencies than of the lower ones. Figure 4.5 depicting ζ_1 versus the transverse shear flexibility parameter reveals that compared to the shearable beam, the classical Euler-Bernoulli beam counterpart overestimates the induced damping. It is also apparent that this trend increases with larger feedback gains. Figures 4.6(a), 4.6(b) and 4.6(c) depict the first three closed-loop eigenfrequencies versus the nondimesional velocity feedback gain K_V, with the transverse shear flexibility ratio E/G' and the nondimensional acceleration feedback gain K_A as

parameters. The results emerging from these figures reveal that for lower frequencies, the incorporation of the velocity feedback control appears to be more efficient than that of the acceleration feedback control. However, as can be concluded from Fig. 4.6(c), for larger mode frequencies, acceleration feedback control is more efficient than the velocity feedback. Figure 4.7 displays the variation of the controlled damping versus the velocity feedback gain K_V, for various values of the feedback gain K_A and of the transverse shear flexibility E/G'. The results reveal that in a certain range of variation of K_V, a linear variation of ζ is experienced. Such a trend was reported also in the paper by Tzou *et al*. (1994). However, at relatively larger values of K_V, a decay in the variation of ζ is observed, decay which is exacerbated when positive acceleration feedback control gains K_A are considered.

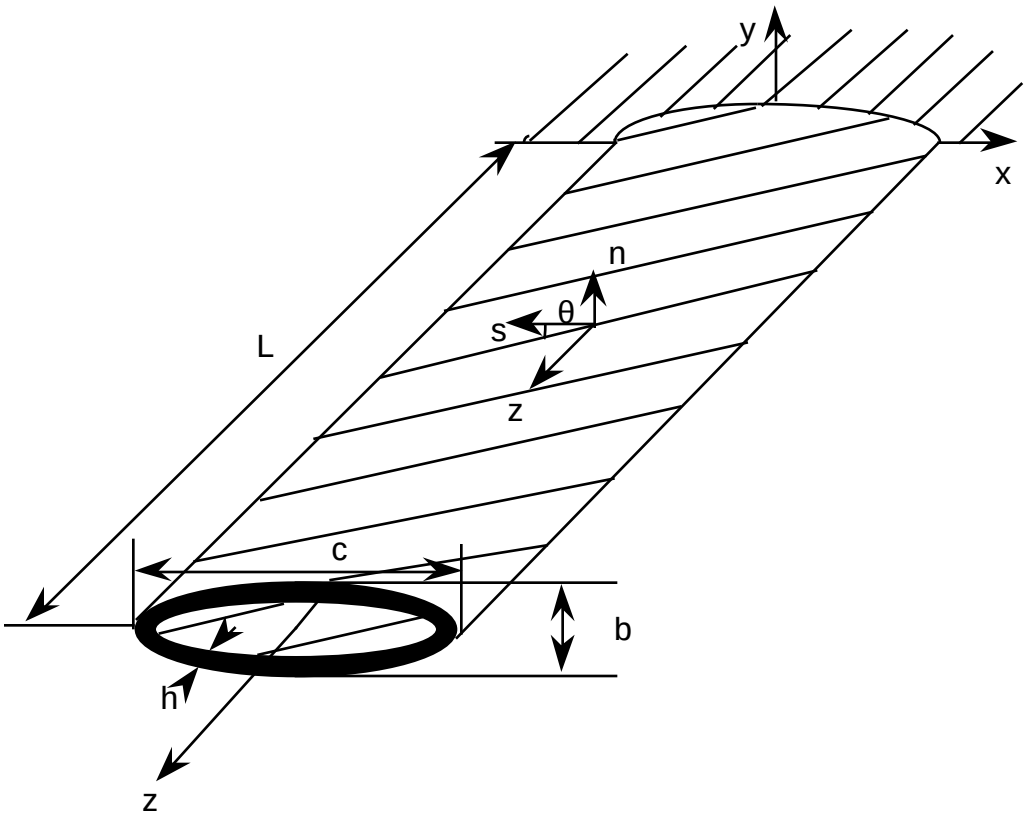

Fig.4.1 Geometry of the Thin-Walled Cantilevered Beam

$c = 10$ in, $b = 2.68$ in, $h = 0.4$ in

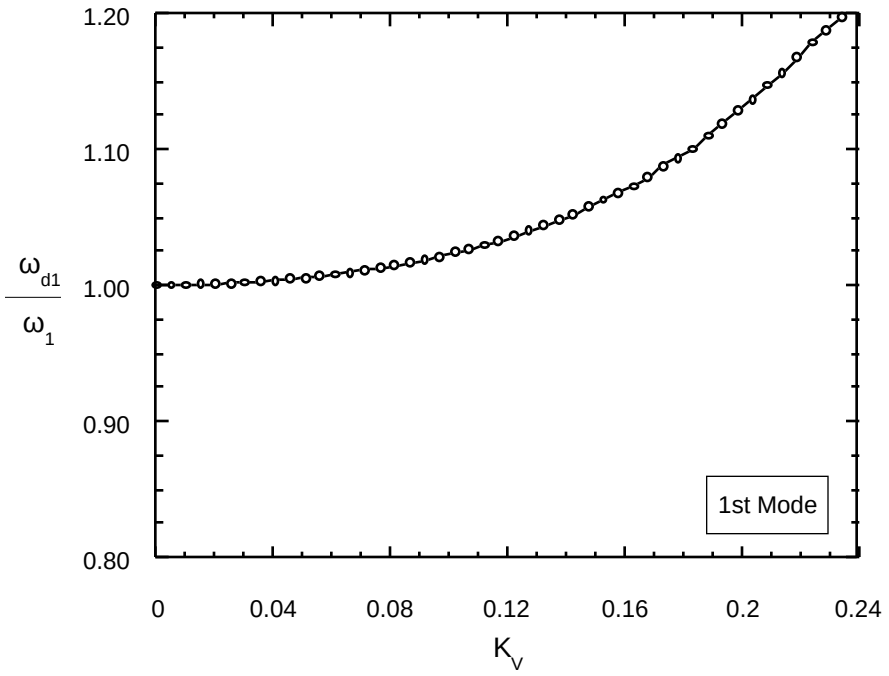

Fig.4.2(a) The first normaliezed damped frequency ω_{d1}/ω_1 versus the dimensionless feedback gain for $AR = 16, \theta = 45^o$ and $\omega_1 = 55.31\ rad/s$

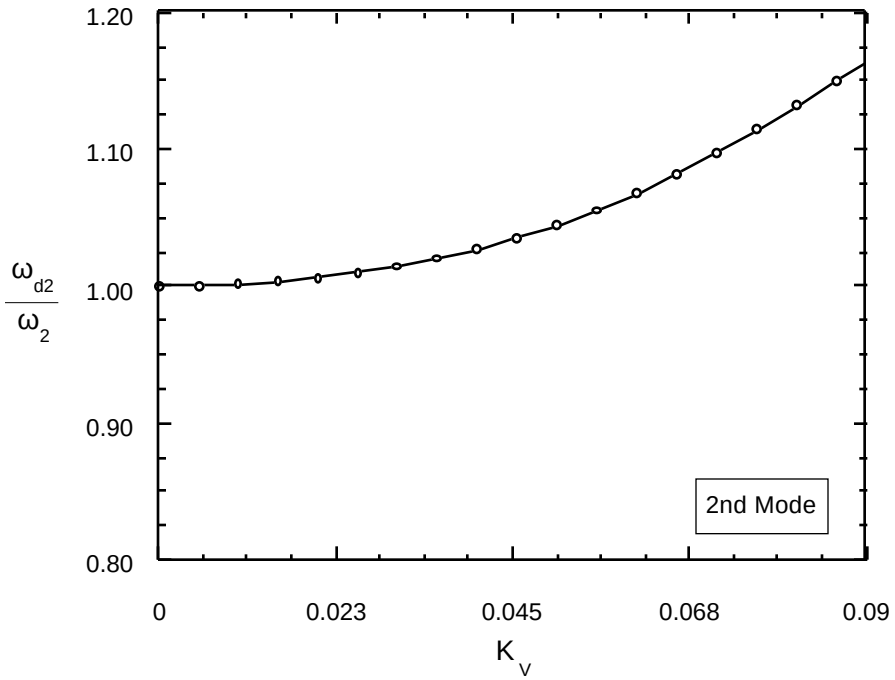

Fig. 4.2(b) The second normalized damped frequency ω_{d2}/ω_2 versus the dimensionlessfeedback gain for $AR = 16, \theta = 45^o$ and $\omega_2 = 345.6\ rad/s$.

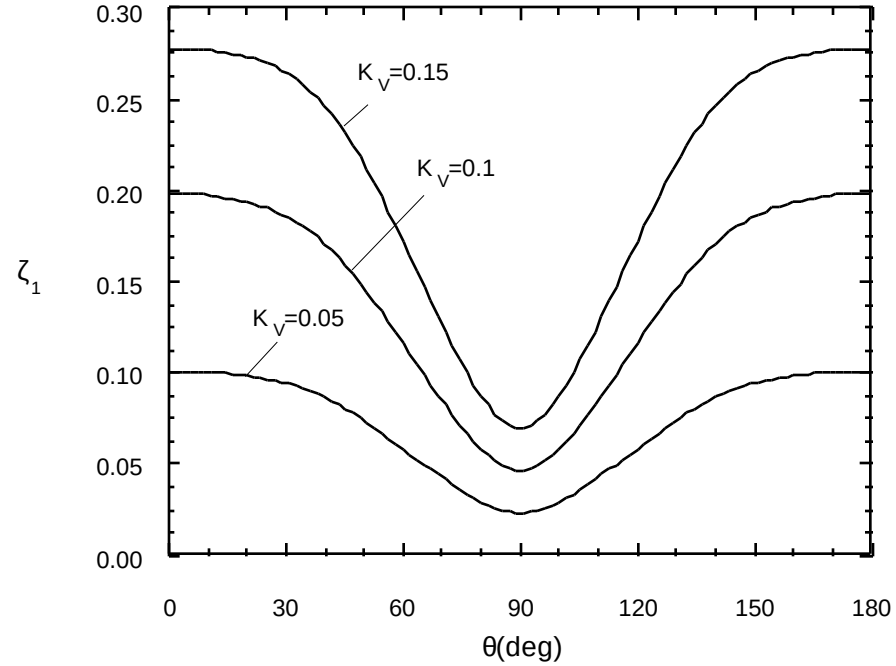

Fig. 4.3 Induced damping factor versus the ply-angle for various values of the feedback gain.

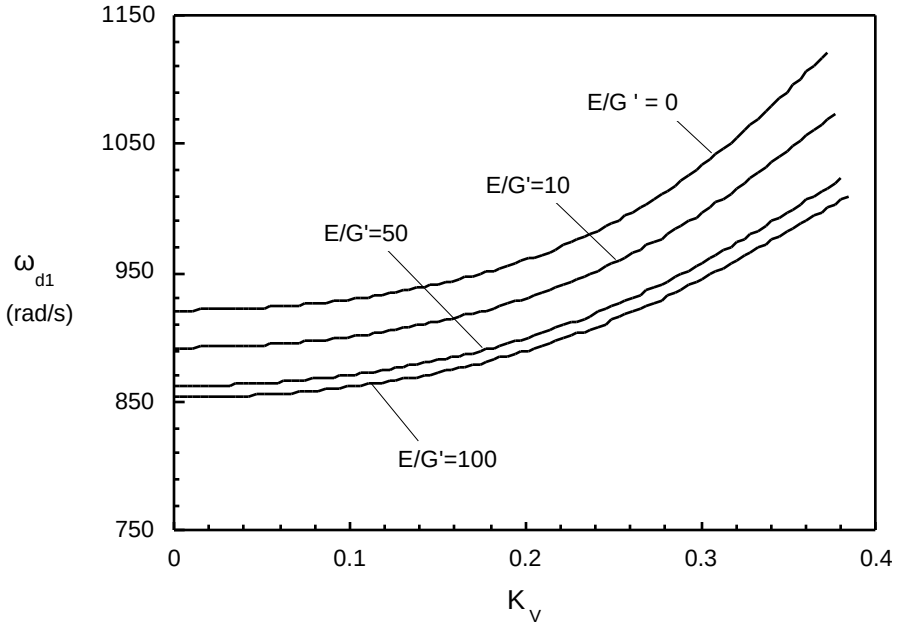

Fig. 4.4(a) The first damped frequency versus the normalized feedback gain for $AR = 6$ and for various transverse shear flexibility ratios.

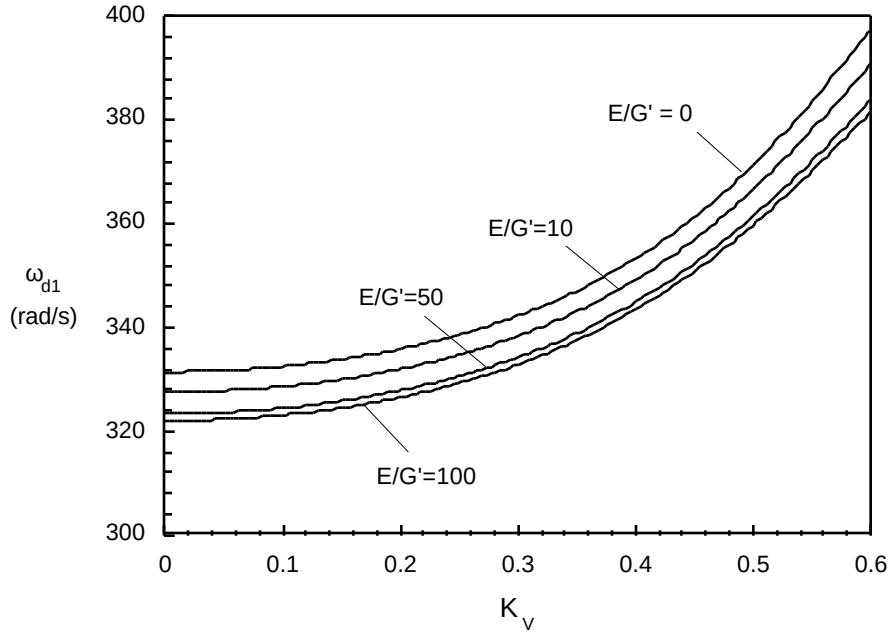

Fig. 4.4(b) The first damped frequency versus the normalized feedback gain for $AR = 10$ and for various transverse shear flexibility ratios.

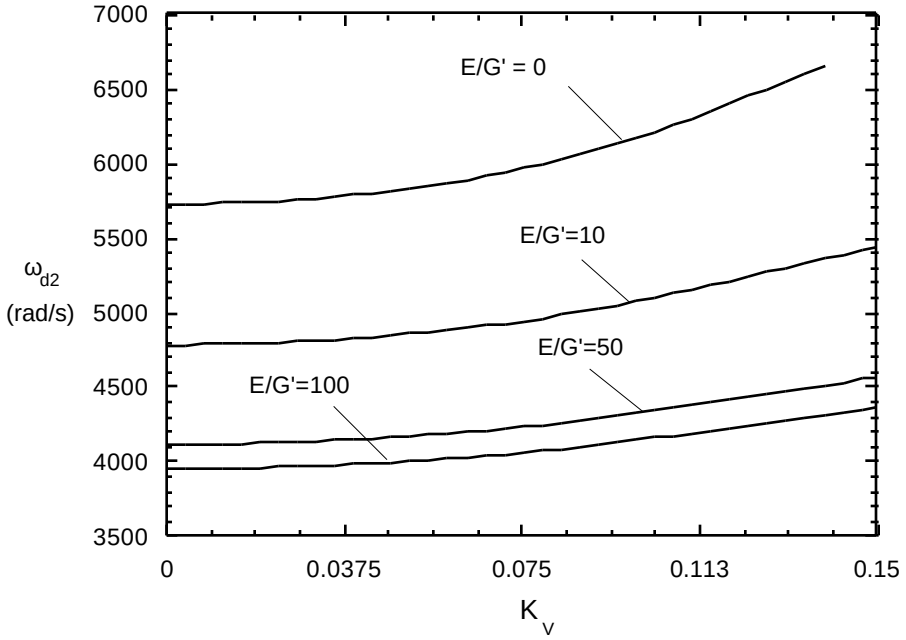

Fig. 4.4(c) The second damped frequency versus the normalized feedback gain for $AR = 6$ and for various transverse flexibility ratios.

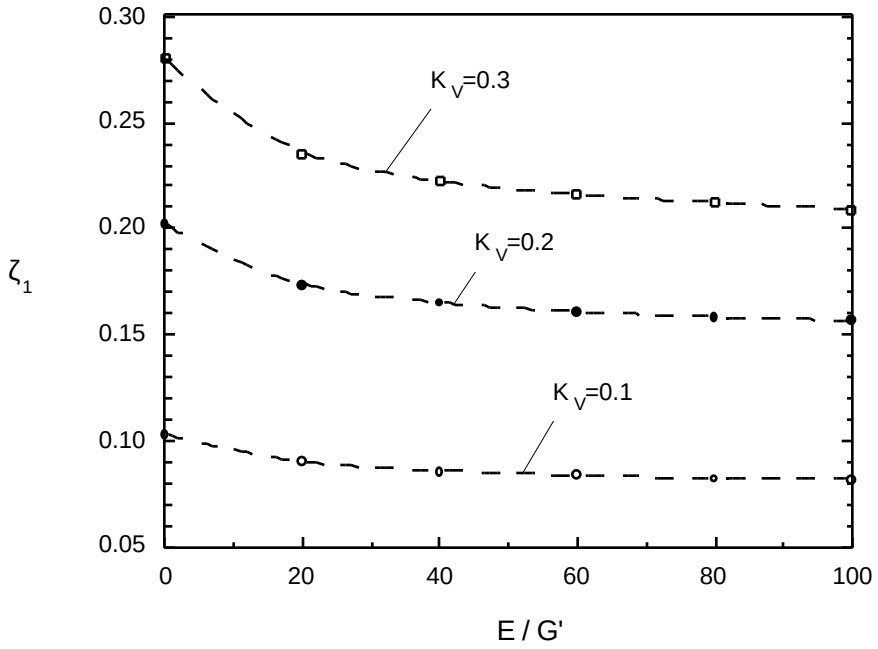

Fig. 4.5 The damping factor versus the transverse shear flexibility ratio for $AR = 6$ and for various values of the feedback gain.

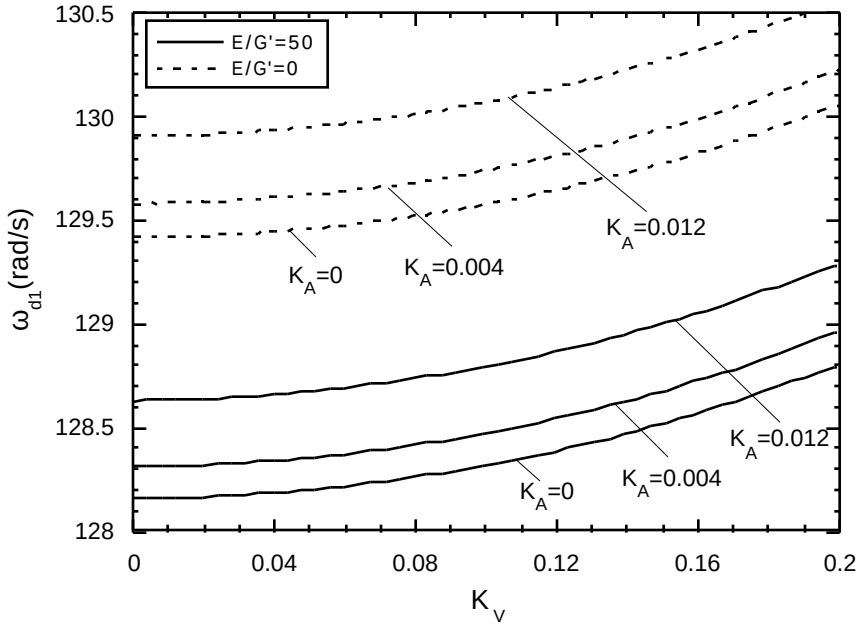

Fig. 4.6(a) The first closed-loop frequency versus the nondimensional velocity feedback gain for $AR = 16$.

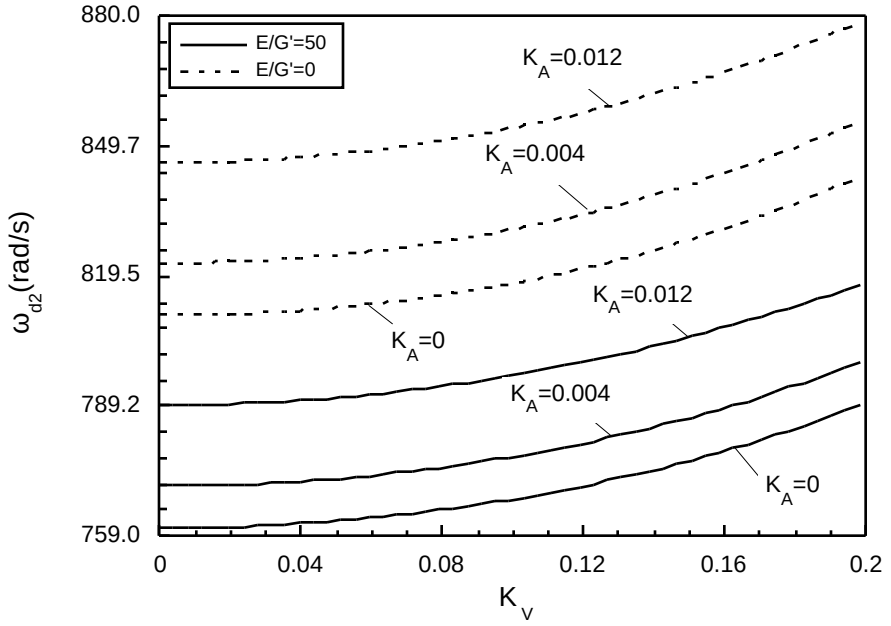

Fig. 4.6(b) The second closed-loop frequency versus the nondimensional velocity feedback gain for $AR = 16$.

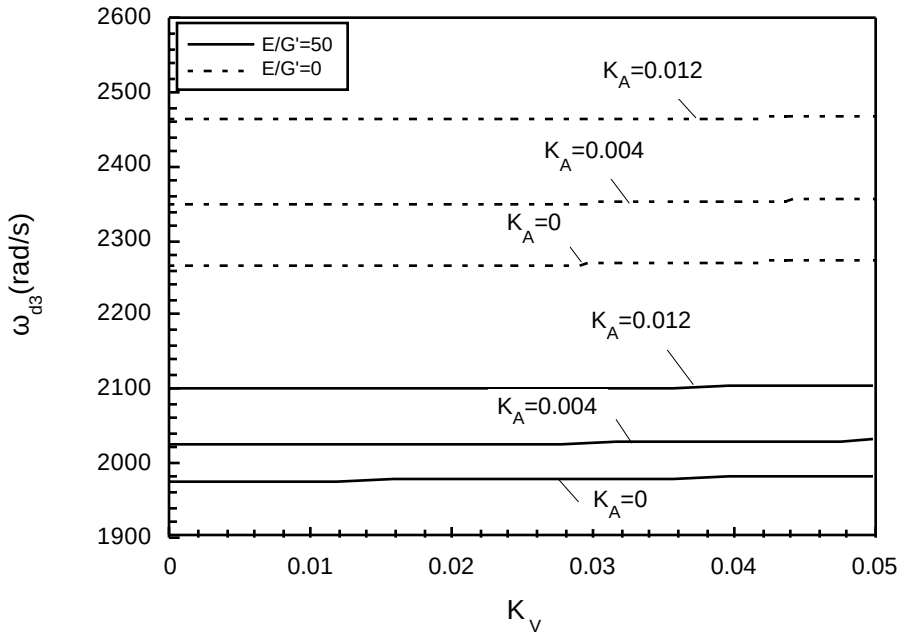

Fig. 4.6(c) The third closed-loop frequency versus the nondimensional velocity feedback gain for $AR = 16$.

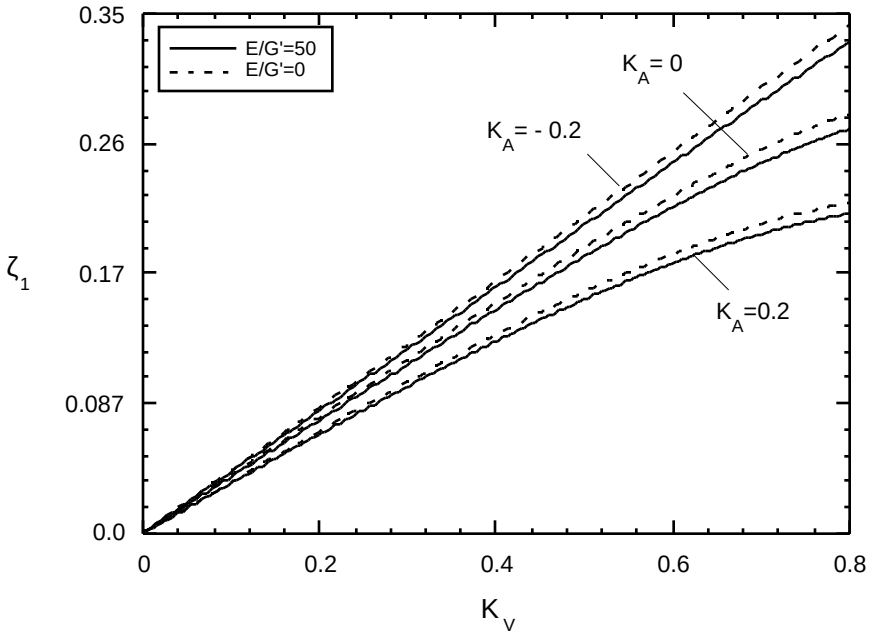

Fig. 4.7 The damping parameter versus the nondimensional velocity feedback gain for $AR = 16$.